LANGMUIR Article
Cite This: Langmuir 2017, 33, 13000-13007 pubs.acs.org/Langmuir

Ferrofluid-Based Droplet Interface Bilayer Networks

Michelle Makhoul-Mansour,[†] Wujun Zhao,[‡] Nicole Gay,[§] Colleen O'Connor,[∥] Joseph S. Najem,[⊥] Leidong Mao,[†] and Eric C. Freeman*[,†]

[†]College of Engineering and [‡]Department of Chemistry, University of Georgia, Athens, Georgia 30602, United States
[§]Department of Genetics, Stanford University, Stanford, California 94305, United States
[∥]College of Engineering and UW Medicine, University of Washington, Seattle, Washington 98195, United States
[⊥]Joint Institute for Biological Sciences, Oak Ridge National Laboratory, and Department of Mechanical, Aerospace and Biomedical Engineering, University of Tennessee, Knoxville, Tennessee 37996, United States

ABSTRACT: Droplet interface bilayer (DIB) networks allow for the construction of stimuli-responsive, membrane-based materials. Traditionally used for studying cellular transport phenomena, the DIB technique has proven its practicality when creating structured droplet networks. These structures consist of aqueous compartments capable of exchanging their contents across membranous barriers in a regulated fashion via embedded biomolecules, thus approximating the activity of natural cellular systems. However, lipid bilayer networks are often static and incapable of any reconfiguration in their architecture. In this study, we investigate the incorporation of a magnetic fluid or ferrofluid within the droplet phases for the creation of magnetically responsive DIB arrays. The impact of adding ferrofluid to the aqueous phases of the DIB networks is assessed by examining the bilayers' interfacial tensions, thickness, and channel activity. Once compatibility is established, potential applications of the ferrofluid-enabled DIBs are showcased by remotely modifying membrane qualities through magnetic fields. Ferrofluids do not significantly alter the bilayers' properties or functionality and can therefore be safely embedded within the DIB platform, allowing for remote manipulation of the interfacial bilayer properties.

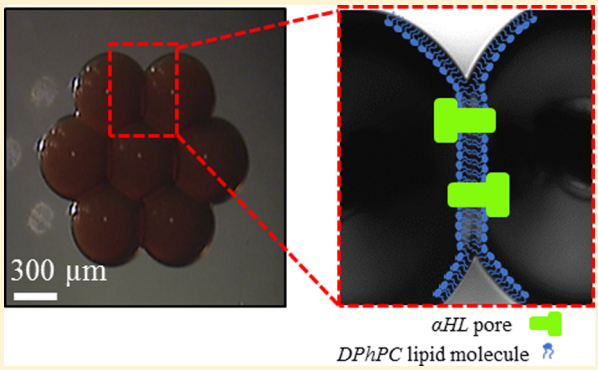

INTRODUCTION

The droplet interface bilayer (DIB) technique has been used for studying membrane transport[1−5] and electrical interrogation of biological membranes.[2,6−11] This platform involves the assembly of model cellular membranes between nanoliter aqueous droplets in an oil environment with lipids dissolved in either phase.[2,12,13] As the droplets are introduced into the oil reservoir, lipid molecules self-assemble in ordered monolayers on the surface of the aqueous droplets.[14,15] When two lipid-coated droplets are brought into contact, a bilayer lipid membrane forms at their interface as shown in Figure 1. While a single DIB may be useful for characterizing the properties of the lipid bilayer and the activity of embedded biomolecules, a prominent advantage of the DIB technique lies in its scalability: multiple droplets may be linked together forming a web of interconnected membranes,[6,16−20] deriving inspiration from the emergent properties of cellular organisms. Current advanced applications of the DIB platform trend toward the tissue-scale, creating vast interconnected droplet structures.[17,21,22] These applications have explored the possibility of using bilayer networks with embedded transporters for purposes such as the fabrication of a microsized half-wave rectifiers[6] or for the evaluation of the collective behavior of lipid bilayers upon the introduction of a pore-inducing peptide.[20]

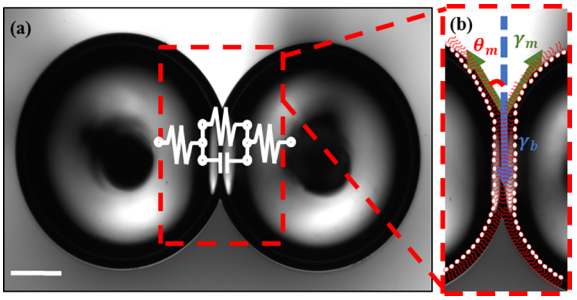

Figure 1. DIB technique. (a) When two nanoliter lipid-coated aqueous droplets are brought together a lipid bilayer membrane is spontaneously formed at the intersection (bar represents 200 μm). This bilayer can be electrically modeled as a capacitor in parallel with a high amplitude resistor. (b) The interfacial tension of the formed bilayer is balanced with the two opposing monolayer tensions at the interfacial area.

These membrane networks are mechanically responsive. Their adhered interfaces are governed by the balance of surface

Received: August 30, 2017
Revised: October 17, 2017
Published: October 18, 2017

DOI: 10.1021/acs.langmuir.7b03055
Langmuir 2017, 33, 13000−13007

tensions at the point of contact[23] (as shown in Figure 1b). The corresponding membrane properties may then be modified by applying mechanical forces or constraints to the droplets,[8] forcing them to adapt a new equilibrium configuration.[24,25] Nevertheless, direct manipulation requires a mechanical path to the droplets of interest—it is not feasible to manipulate droplets at the center of a cluster through traditional methods without jeopardizing the structural integrity of the whole. Thus, a contact-free methodology for manipulating selected droplets within the structures is necessary.

Remote actuation of droplets may be achieved through many different techniques: electrowetting,[26] wetting gradient,[27] thermal gradient,[28] vibrations,[29] dielectrophoresis,[26,30,31] and magnetophoresis.[32,33] Out of these options, electrowetting and dielectrophoresis have been successfully combined with the DIB technique.[30,31] However, as the volume fraction of the droplets increases, these techniques become less appealing, as all aqueous droplets will respond in a similar fashion to the external field. To counter this, the droplets must be selectively imbued with sensitivity to the manipulation mechanisms.

Magnetophoresis provides an optimal combination of flexibility and selectivity, may be achieved with simple magnets, and does not require specialized electrodes or substrates. Most organic materials exhibit negligible variations in magnetic susceptibility,[34,35] and consequently only droplets imbued with a magnetic susceptibility within a DIB network will perceptibly respond to an externally supplied magnetic field. Earlier works have demonstrated the potential uses of magnetic manipulation within the DIB technique by incorporating magnetic beads within the droplets[16] and using permanent magnets to guide the construction of 3D droplet networks. Unfortunately, these beads behave as a solid contained within the droplets, posing limitations to the incorporation of these magnetically imbued droplets within microfluidic chips or larger DIB structures. Such limitations may be circumvented through the use of magnetic fluids or ferrofluids.

Ferrofluids consist of stable colloidal suspensions of magnetic nanoparticles (such as maghemite Fe_2O_3 or magnetite Fe_3O_4) coated with a suitable surfactant and dispersed within a carrier fluid. The size of the nanoparticles used in ferrofluids is small enough to cause these materials to behave as macroscopically continuous liquids. When applying an external magnetic field, the dispersed nanoparticles within the carrier fluid align themselves with the field producing a magnetic response. Once the external field is removed, Brownian motion rapidly scatters the nanoparticle orientation, eliminating any permanent magnetization and rendering the fluid superparamagnetic.

Contact-free manipulation and assembly of the droplet networks can be achieved by incorporating ferrofluids within the DIB platform. However, there is a risk of competition between the nanoparticles, stabilizing surfactants, and lipids at the oil−water interfaces. In this work, the qualities of DIBs are assessed to ensure that the lipid membrane functionality is retained as ferrofluids are introduced. This is achieved by measuring lipid bilayer's specific capacitance, tension, thickness, and energy of adhesion, then comparing the values for DIBs that have been formed with and without the use of ferrofluids. Next, the response of these membranes to the presence of a pore-forming toxin such as alpha-hemolysin is assessed. Finally, magnetic control of membrane dimensions is showcased as a proof-of-concept for remote manipulation of the DIB structures.

MATERIALS

Lipid-in-Oil Solutions. The lipid-out method for DIB formation is used in this work, where lipids are dissolved in the oil phase. Zwitterionic lipids (1,2-diphytanoyl-*sn*-glycero-3-phosphocholine (DPhPC), Avanti Polar Lipids, Alabaster, AL) were suspended in a 1:1 (volume:volume) mixture of Hexadecane and Silicone Oil AR20 (both Sigma-Aldrich, St. Louis, MO) at a concentration of 0.5 mg/mL unless stated otherwise. All lipid solutions were sonicated for 80 min (Avanti Sonicator, Avanti Polar Lipids, Alabaster, AL) and afterward stored at 2 °C.

Ferrofluid Solutions. *Synthesis and Characterization of Ferrofluids.* Ammonium hydroxide solution (28%), iron(II) chloride tetrahydrate (99%), iron(III) chloride hexahydrate (97%), nitric acid (70%), iron(III) nitrate nonahydrate (98%), and sodium hydroxide (98%) (all purchased from Sigma-Aldrich, St. Louis, MO) were used as received from the vendor. Maghemite nanoparticles were produced using a chemical coprecipitation method.[36] Typically, 50 mL of ammonium hydroxide solution was added into a mixture of 100 mL of 0.4 M iron(II) chloride tetrahydrate and 0.8 M iron(III) chloride hexahydrate, then stirred at room temperature for 30 min. The suspension was centrifuged at 2000 × *g* for 3 min, and the obtained precipitate was dispersed in 200 mL of 2 M nitric acid and 0.35 M iron(III) nitrate nonahydrate and kept at 90 °C for 1 h. During this time, the color of the mixture changed from black (Fe_3O_4) to reddish brown (Fe_2O_3). The maghemite nanoparticle suspension was further centrifuged at 3000 × *g* for 3 min and finally dispersed in 120 mL of deionized (DI) water, resulting in a stable dispersion with a pH of 1.5−2. 40 mL of Atlox 4913 (Croda, Edison, NJ), a graft copolymer solution, was added to the dispersion before raising pH to 7.0. The dispersion was then stirred for 1 h, and the resulting ferrofluid was dialyzed (using a dialysis membrane purchased from Spectrum Laboratories, Rancho Dominguez, CA) against DI water (refreshed every 24 h) for 1 week. Excess water was vaporized afterward at 72 °C. Morphology and size of nanoparticles were characterized via transmission electron microscopy (TEM; FEI, Eindhoven, The Netherlands; Figure 2). Using a vibrating sample magnetometer

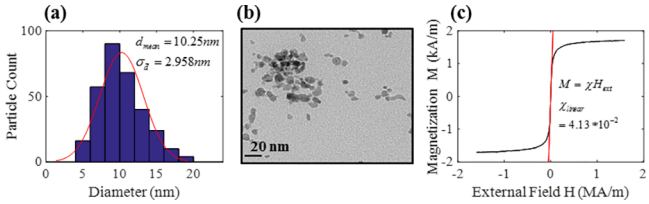

Figure 2. (a) The size distribution of maghemite nanoparticles within the ferrofluid showed a mean particle size of 10.250 nm with a standard deviation of 2.958 nm. (b) A transmission electron microscopy (TEM) image of the nanoparticles. Scale bar represents 20 nm. (c) Magnetization curve for the ferrofluid: given a known bulk magnetization of maghemite (370 kA/m) and a saturation magnetization (from curve) of 1.71 kA/m, the concentration of magnetic particles within the ferrofluid was estimated to be at 0.46% by volume. The ferrofluid exhibits no hysteresis and is superparamagnetic. The linear magnetic susceptibility shown as the red dashed line prior to saturation is 0.0413.

(VSM; MicroSense, Lowell, MA) with a 2.15 T electromagnet, magnetic properties of the ferrofluid were measured (at room temperature). The magnetic moment of ferrofluid was measured over a range of applied fields from −20 to +20 kOe (all measurements were conducted in step field mode with a step size of 250 Oe/s).

Ferrofluid Solutions for DIBs. The ferrofluid solutions used in this work are stable aqueous suspensions of magnetite (γ-Fe_2O_3) as described previously at a nanoparticle concentration of 0.46% by volume. 250 mM Potassium Chloride (KCl, Sigma-Aldrich, St. Louis, MO) and 10 mM 3-(N-morpholino) propanesulfonic acid (MOPS, Sigma-Aldrich, St. Louis, MO) salts were added to the ferrofluid solution. Solutions were systematically sonicated prior to each use. In

DOI: 10.1021/acs.langmuir.7b03055
Langmuir 2017, 33, 13000−13007

the experiments involving α-hemolysin (αHL) pores, the same ferrofluid solution mentioned here was used with the addition of 1 M KCl and 10 mM of trihydrochloride (Tris-HCl, Molecular Biology grade- Promega Corporation, Madison, WI) instead. A concentration of 1.25 μg/mL of wild-type Alpha-Hemolysin (αHL) from *Staphylococcus aureus* (Sigma-Aldrich, St. Louis, MO) was then added to the solution before being stored at a temperature of 2 °C.

Aqueous Buffer Solutions for DIBs. An aqueous buffer solution was prepared by adding 250 mM KCl and 10 mM MOPS resulting in a pH of 6.98. This solution was used in all experiments except for the ones involving αHL where a 10 mM Tris-HCl, 1 M KCl buffer solution (pH 7.0, as measured) was used.

PDMS Dishes. Polydimethlysiloxane (PDMS) mixtures were created from SYLGARD 184 Silicone Elastomer Base (Dow Corning Corporation, Midland, MI) with a 13:3 v:v ratio of base to curing agent. The solution was degassed in a vacuum oven for 15 min and then poured into molds and cured at 80 °C for 90 min.

Magnetowetting Substrate. PDMS mixtures were poured into long cylindrical tubes 5 mm in diameter with a flat plane carved one side for visibility. A 1.1 mm O.D. glass capillary (World Precision Instruments, Sarasota, FL) was inserted lengthwise into the center of the tube to form a well, and the PDMS was cured in a vacuum oven (VWR, Radnor, PA). The cured PDMS cylinder containing the well was broken into smaller sections, and the glass capillary was removed to create the central channel. A perpendicular channel was punched into the PDMS tube, orthogonally intersecting the central channel. The perpendicular channel and base of the central channel was filled with uncured polyethylene glycol dimethacrylate hydrogel (PEG-DMA, Polysciences Inc., Bucks County, PA) containing Irgacure (Sigma-Aldrich, St. Louis, MO) as a photoinitiator. A silver−silver/chloride (Ag/AgCl) electrode (0.125 mm in diameter, GoodFellow, Coroapolis, PA) was threaded into the liquid hydrogel, and the gel was solidified by exposure to a high intensity UV LED (Thorlabs, Newton, NJ) for 3 min. The whole substrate was then adhered to a glass coverslip for stability. The final substrate (Figure 3) provides a compact encapsulated platform for investigating magnetowetting.

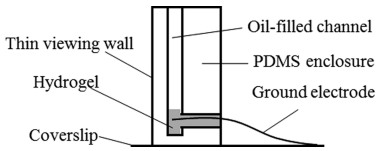

Figure 3. Sketch of the PDMS substrate used for magnetowetting measurements. The vertical channel is approximately 1.1 mm in diameter.

METHODS

Creation of Magnetic Droplet Interface Bilayer Networks. Glass capillary tubes (KWIK-Fil Borosilicate Glass Capillaries, World Precision Instruments, Inc., Sarasota, FL; reported dimensions: 100 mm in length, 1.0 mm in outer diameter, and 0.58 mm in inner diameter) were pulled to fine points using a programmable pipet puller (P-1000, Sutter Instruments, Novato, CA) with pretested settings for the pulling force, the chamber temperature, and the holding time. The final inner diameter of the needle apertures was measured to be around 30 μm. These needles were then filled with either the aqueous buffer or ferrofluid solution using 34G microfils (World Precision Instruments, Sarasota, FL) and were attached to microinjectors (Sutter Instruments, Novato, CA) mounted on manual micromanipulators (Siskiyou, Grants Pass, OR). The PDMS well substrate was placed on the stage of a zoom microscope (Nikon SMZ1000, Tokyo, Japan) and filled with the lipid-oil solution. Droplets were systematically injected in the oil reservoir using a pressure-operated injector (FemtoJet 4i, Eppendorf) with specified injecting pressures and holding times to produce droplets with the desired diameters for each solution. After sufficient time for monolayer formation, a permanent magnet (neodymium (NdFeB) magnet, K&J Magnetics, Inc.) was gradually brought closer to the dish containing the droplets. For cases containing only ferrofluid droplets, the magnet pulled the ferrofluid droplets into contact at a single location and the DIB networks were readily formed. Upon the removal of the magnet, the droplets remained adhered in a structured membrane network. For the case where DIB networks are formed using a combination of both ferrofluid and water droplets, a permanent magnet mounted on a 3-axis manipulator (Siskiyou, Grants Pass, OR) was used to the move the ferrofluid droplets through the medium to gradually recruit the water droplets into a larger structure.

Measurement of Interfacial Tensions. Surface tensions of lipid monolayers formed at the oil−water and oil-ferrofluid interfaces were evaluated using the pendant drop method.[13,37] In this technique, the interfacial tension (IFT) of a fluid−fluid interface is determined from a digitized series of images acquired for a suspended pendant drop of one of the liquid phases (here water or ferrofluid) formed at the tip of a needle and submerged in the second phase (here the lipid−oil mixture). These images are then used to evaluate the IFT with an accuracy of ±0.1 mN/m[38−41] through a Python-based curve-fitting process of the drop edge coordinates.[37,42] A simple experimental system was used for the pendant-drop tensiometry as shown in Figure 4a. The diffused light of a Quartz Tungsten-halogen lamp (QTH10/M

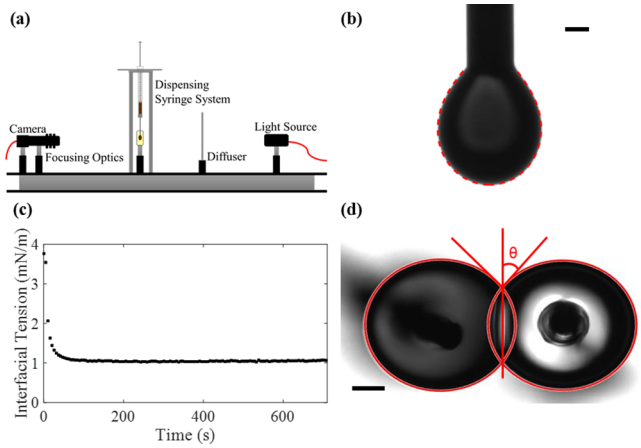

Figure 4. (a) Schematic representation of the pendant drop experiments for the measurement of interfacial surface tension. The diffused light of a halogen lamp passes through a Quartz cuvette filled with 3 mL of the lipid-oil mixtures in which a water or ferrofluid droplet is dispensed from a clean steel needle. Images are acquired through a CCD camera equipped with a zoom lens. (b) Acquired images of the droplets were analyzed using the open-source OpenDrop software. The interfacial tension was obtained through a curve-fitting process of the drop edge coordinates. (c) A typical measurement of the monolayer tension for a ferrofluid droplet in a lipid-in-oil mixture (DPhPC dissolved in a 1:1 (v: (v) solution of hexadecane and silicone oils in a concentration of 0.5 mg/mL) shows that the interfacial tension decreases rapidly upon droplet formation in the lipid-oil. The steady-state tension value obtained from these measurements was used to calculate the bilayer tension using eq 1. (d) The membrane's area, length, and external contact angle were found for each analyzed bilayer using a MATLAB code for image analysis. Droplets were fitted to circles and geometric relations were used to derive the interfacial area and angle of contact.

- Quartz Tungsten-Halogen Lamp, M4 Tap, Thorlabs, Newton, NJ) passes through a Quartz cuvette (10 mm cuvette cell spectrometer open top, Science Outlet, Tsuenwan, Hong Kong) filled with 3 mL of the lipid−oil mixtures in which a water or ferrofluid droplet is dispensed from a clean 30 G steel needle (Harvard Apparatus, Holliston, MA). Images are captured using a CCD camera (high sensitivity DCC1240C, Thorlabs, Newton, NJ) to which zoom lenses (6.5X zoom lenses with a 0.7−4.5× magnification range, Thorlabs, Newton, NJ) were attached through a mount adapter (MVLCMC - C-

DOI: 10.1021/acs.langmuir.7b03055
Langmuir 2017, 33, 13000−13007

mount adapter for zoom lens extension tubes, Thorlabs, Newton, NJ). In order to prevent any wetting that might occur at the tip of the needle, clean wipes (Kimwipe, Kimberly-Clark Professional, Roswell, GA) were used to remove any water or ferrofluid residual before droplets were formed.

Measurements of DIB Specific Capacitance, Adhesion Energy, and Thickness. As shown in Figure 1a, a DIB can be electrically approximated as a capacitor in parallel with a high amplitude resistance.[2,5] Since the membrane resistance is often in the order of GΩ,[2,43] the resistive current is often ignored or compensated for, and the overall current of a bilayer simplified to its capacitive component. This capacitance may then be estimated by measuring the current necessary for charging the membrane to a prescribed voltage. Normalizing this capacitance with respect to area allows for a quick diagnostic of bilayer thickness, configuration, and integrity.[9−11]

The area of the membrane is governed by the balance of IFTs at the monolayer−bilayer annulus as depicted in Figure 1b. Upon formation, the membrane expands until the tensions at the annulus are balanced.[9,44,45] The equilibrium relationship between the bilayer tension γ_b and the two opposing monolayer tensions γ_m deviating from the normal plane by an angle of contact θ is given by

$$\gamma_b = 2\gamma_m \cos\theta \tag{1}$$

The contact angle depends on the balance of the interfacial tensions and will remain constant in the absence of any external constraints,[7,8,46] and is directly related to the minimization of interfacial energies for the two droplets.[35] The bilayer tension can therefore be found for a given combination of measured monolayer tensions and contact angles for a membrane at equilibrium. These two tensions will allow for the evaluation of the bilayer's adhesion energy also referred to as membrane's free energy of adhesion ΔF:[45]

$$\Delta F = 2\gamma_m - \gamma_b = 2\gamma_m(1 - \cos\theta) \tag{2}$$

The energy of adhesion is directly linked to the interactions of the two surfactant monolayers;[47,48] consequently, it is a reliable point of comparison for membranes with similar oil/lipid compositions. As the monolayers draw together from infinity to the equilibrium membrane distance h_e, the energy is reduced by the integrated disjoining pressure Π summing the combined steric, electrostatic, and van der Waals force interactions between the lipid tails. This is equivalent to the energy of adhesion as defined above, and characterizes the favorability of the adhered film.[14,15,49]

$$\gamma_b = 2\gamma_m - \int_{\infty}^{h_e} \Pi \, dh \tag{3}$$

$$\Delta F = \int_{\infty}^{h_e} \Pi \, dh \tag{4}$$

The equilibrium thickness of the membrane may be characterized by its specific capacitance C_m. Knowing that C_m varies with the amount of solvent remaining in the bilayer's hydrophobic region,[9,44,50,51] results obtained for different types of DIBs suggest the amount of residual oil remaining within the bilayer. It has also been established that C_m is related to the thickness of the bilayer's hydrophobic region D_C as well as its dielectric permittivity ε_r[50,52] with ε_0 representing the permittivity of vacuum. For the following calculations, we assumed the value of ε_r to be equal to that of long-hydrocarbon chain molecules (2.2[9,53]). It should be noted that D_C is not necessarily the equilibrium film thickness h_e. Both D_C and C_m values allow for quantification of any induced effect (or the lack thereof) when the magnetic nanoparticles are incorporated into the DIB technique.

$$C_m = \frac{\varepsilon_r \varepsilon_0}{D_C} \tag{5}$$

Droplets (~300 μm radius) were deposited on agarose (2% by weight EZ Pack Agarose LE, Molecular Biology grade, Benchmark Scientific, Sayresville, NJ) coated silver/silver chloride electrodes (125 μm in diameter, GoodFellow, Coroapolis, PA). Each electrode was mounted on a three-axis manual micromanipulator (Siskiyou, Grants Pass, OR) for control over the droplet positions and electrode manipulation. All electrical measurements (membrane capacitance as well as channel recordings) were recorded in voltage clamp mode (Whole Cell $\beta = 1$) using the Axopatch 200B patch clamp amplifier and the Digidata 1550 data acquisition system (Molecular Devices, Sunnyvale, CA) at a sampling frequency of 5 kHz and filtered at 1 kHz (using the embedded low-pass Bessel filter −80 dB/decade). The nominal capacitance of the bilayers was evaluated using a 40 Hz, 10 mV AC triangular wave (33120A function generator, Hewlett-Packard, Palo Alto, CA). Stray capacitances arising from any residual capacitance in experiment was accounted for by using the patch-clamp amplifier's built-in whole-cell capacitance compensation before making any measurements. The value of the bilayer's capacitance was obtained using a MATLAB code from the recorded square wave current response and the corresponding applied voltage. For each analyzed case, an image of the DIB was taken through the inverted microscope using a CCD camera (DFC365 FX, Leica, Wetzlar, Germany) once the bilayer was given enough time to form and stabilize. These images were exported and analyzed using a MATLAB code that fits the droplets into circles and uses geometric equalities to derive the bilayer area and angle of contact as illustrated in Figure 4d using a calibrated pixel-micron value from the microscope software.

The bilayer formed between the droplets was characterized by the visible intersecting chord on the inverted microscope, assuming that the membrane exhibits minimal ellipticity due to gravitational effects. The nominal specific capacitance C_m was evaluated for each different case using the values obtained from the bilayer's capacitance and area measurements. Droplets with a radius of 300 μm and an assumed surface tension of approximately 1 mN/m[44] provide a Bond number on the order of 0.01 as shown in eq 6, minimizing gravitational effects for this particular oil−water combination where the density difference is 110 kg/m^3. Here $\Delta\rho$ is the difference in density between the two phases, g is the gravitational constant, R is the radius of the droplet, and γ_m is the monolayer surface tension.

$$B_O = \frac{\Delta\rho g R^2}{\gamma_m} \tag{6}$$

αHL Functionality. αHL obtained from *Staphylococcus aureus* bacteria is a mushroom-shaped, homo-oligomeric, transmembrane, pore-forming toxin[54,55] that acts as a natural lysis inducing agent. With a well-known structure and electrical characterization of the pore,[1,54−57] αHL insertion activity was used here as a tool to assess the functionality of the ferrofluid-based DIBs. The behavior of the pore-forming toxin (PFT) was examined in four different cases: a control case with two water droplets, a case with two ferrofluid droplets, and mixed water-ferrofluid DIB cases with alternating droplet locations. In all cases, αHL was inserted from the reference side of the membrane. The obtained current traces with a DC applied voltage of 50 mV were recorded in voltage-clamp mode (Whole Cell $\beta = 1$) at a sampling frequency of 5 kHz and filtered at 1 kHz using a low-pass Bessel filter (−80 dB/decade). Post-acquisition, a 500 Hz fourth-order Butterworth low-pass filter was applied in MATLAB when plotting the obtained current traces.

Magnetowetting. The magnetowetting substrate channel described previously was filled with the oil-lipid solution, forming a lipid monolayer on the hydrogel surface at the bottom of the channel. A 1.1 mm diameter ferrofluid droplet was deposited at the channel entrance using the same protocol from the formation of magnetic DIB networks and allowed to gradually descend through the channel due to gravitational forces, accumulating a lipid coating as it descended from the surrounding oil. Upon contacting the hydrogel at the bottom of the channel, a droplet-hydrogel bilayer (DHB) formed spontaneously between the gel and the ferrofluid droplet. A Ag/AgCl electrode (125 μm in diameter- GoodFellow, Coroapolis, PA) was then inserted into the ferrofluid droplet from above using a three-axis manual micromanipulator (Siskiyou, Grants Pass, OR), providing electrical characterization of the DHB through the ground electrode placed in the hydrogel support. These electrodes were connected to a Multiclamp 700B patch clamp amplifier and the Digidata 1550 data

DOI: 10.1021/acs.langmuir.7b03055
Langmuir 2017, 33, 13000−13007

acquisition system (Molecular Devices, Sunnyvale, CA) and the capacitance of the membrane was measured using the same protocol from the previous measurements of bilayer capacitance, calculating the area of the membrane through the obtained specific capacitance values for ferrofluid-buffer combinations. A permanent magnet was placed on a translating stage (PT1/M single axis translation stage with standard micrometer, Thorlabs, Newton, NJ) underneath the slide and gradually moved closer to the substrate in 1 mm increments using the micrometer, increasing the strength of the exerted magnetic field and causing the interfacial membrane between the ferrofluid droplet and the hydrogel support to expand. Visualization of the droplet in the channel was achieved through an inspection microscope with a CCD camera (Motic, Hong Kong).

RESULTS AND DISCUSSION

Creation of Ferrofluid-Enabled Droplet Interface Bilayer Networks. Ferrofluid droplets were easily assembled into larger DIB structures through the introduction of an external magnetic field as described previously. The droplets were dispersed within the oil, and a permanent magnet was used to bring the droplets into contact. The magnet was removed after membrane formation, and the structure remained in place even in the absence of a magnetic field. These structures are stable and allow for the combination of water and ferrofluid droplets in DIB clusters as shown in Figure 5.

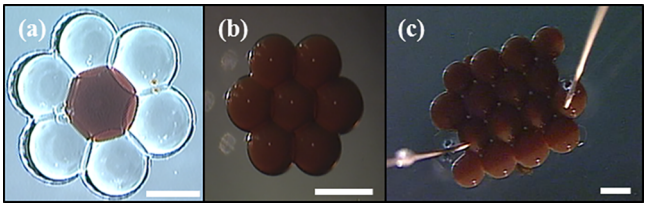

Figure 5. Use of ferrofluid nanoliter droplets for the fast and easy construction of 2D DIB structures. In panel a, a single ferrofluid droplet previously introduced to a lipid−oil reservoir was controlled with an external magnet to gradually recruit additional droplets into a hexagonal-shaped DIB cluster. The end result was a stable DIB network that included both aqueous and ferrofluid droplets. Meanwhile, in the cases where exclusively ferrofluid droplets were used, as shown in panels b and c, a quick and automatic self-assembly of the networks was induced through a permanent magnet: as the magnet was brought closer to the lipid−oil dish, the lipid-coated ferrofluid droplets were pulled into contact with each other and the lipid bilayers formed spontaneously. Once the magnetic source was removed, the networks preserved their structural integrity, and the droplets remained in contact. Scale bars represent 750 μm.

Measurement and Comparisons of Ferrofluid DIB Specific Capacitance, Tension, Adhesion Energy, and Thickness. Table 1 shows the average values and standard deviations for the obtained equilibrium monolayer and bilayer tensions (resting bilayer tension obtained when no additional external mechanical force is being applied to the droplets), external contact angle, specific capacitance, and thickness and energy of adhesion of bilayers formed for DIBs with and without ferrofluids. The results show that the obtained values for each of the bilayers' properties are similar, indicating that the incorporation of ferrofluids within the aqueous phase does not influence the properties of the formed lipid bilayers. While it is possible that the surrounding monolayer is a mixture of both the phospholipids and excess ATLOX surfactant, any excess ATLOX is wicked away from the bilayer membrane during formation as shown by Jeong et al.[58] Consequently, the underlying structure of the bilayer appears unchanged. This may be further validated by observing the behavior of pores and channels within the membrane

αHL Functionality in Ferrofluid DIBs. To determine whether αHL is still functional in ferrofluid DIBs, we examined the formation of conductive pores in various combinations of water and ferrofluid droplets. A total of 96 αHL insertion events (22 insertion events from the configuration shown in Figure 6a, 27 from panel b, 22 from panel c, and 25 from panel d) were examined. The corresponding single pore conductance ranged between 0.379 and 1.258 nS (with a total average of 0.866 nS and a standard deviation of 0.202 nS). In all cases, the measured single pore conductances fell within previously reported ranges for αHL,[57,59] demonstrating that functional peptide pores can still be embedded with ferrofluid DIBs. The variance in pore conductance is largely due to the structural difference of αHL. The αHL pore is formed by self-organizing heptameric monomers; however, the existence of several stable hexamer oligomeric structures that can be inserted into the lipid bilayer is highly probable and well supported by previous studies.[57,59] As depicted in Figure 6b,c,d, potential blocking events occur when the ferrofluid droplets are used. However, despite the occurrence of these blocking events, the PFT is still functional within these bilayers, and thus can be used in larger DIB structures involving magnetically responsive droplets.

Ferrofluids for the Formation of DHBs and Magneto-wetting. The successful incorporation of ferrofluids within the DIB platform allows for manipulation of select droplets through a magnetic field. Similar to the regulated attachment method,[60] this allows for indirect control over the membrane dimensions as shown in Figure 7, plotting the change in membrane area against the magnetic Bond number B_M. This quantifies the impact of the magnetic body force relative to the interfacial tension force[61,62] (eq 7). In this case, the tension of the droplet-oil interface is very low (Table 1), and this dimensionless number quickly increases upon exposure to a permanent magnet.

$$B_M = \frac{\mu_0 \Delta\chi {H_{ext}}^2 \mathrm{Vol}^{1/3}}{2\gamma_m} \quad (7)$$

Here μ_0 is the permeability constant ($4\pi \times 10^{-7}$), $\Delta\chi$ is the difference in magnetic susceptibilities between the ferrofluid and oil (Figure 2), H_{ext} is the intensity of the applied magnetic field, Vol is the droplet volume (~500 nL), and γ_m is the surface tension of the ferrofluid droplet taken from Table 1 (1.19 mN/m). The ferrofluid droplet is flattened upon exposure to a magnetic field, increasing its interfacial area as depicted in Figure 7. As the magnet is brought gradually closer to the channel substrate, the droplet shifts from a half-sphere to

Table 1. Measurements Obtained for DIBs with and without Ferrofluids at 22 °C

type	C_m (μF/cm^2)	γ_m (mN/m)	γ_b (mN/m)	$2\theta_m$(deg)	D_c (Å)	ΔF (mN/m)
water (n = 13)	0.553 (±0.094)	1.113 (±0.174)	1.958 (±0.300)	60.219 (±5.783)	33.786 (±7.577)	0.267 (±0.064)
ferrofluid (n = 11)	0.583 (±0.030)	1.119 (±0.151)	1.936 (±0.241)	59.365 (±1.311)	32.002 (±1.802)	0.291 (±0.038)

DOI: 10.1021/acs.langmuir.7b03055
Langmuir 2017, 33, 13000−13007

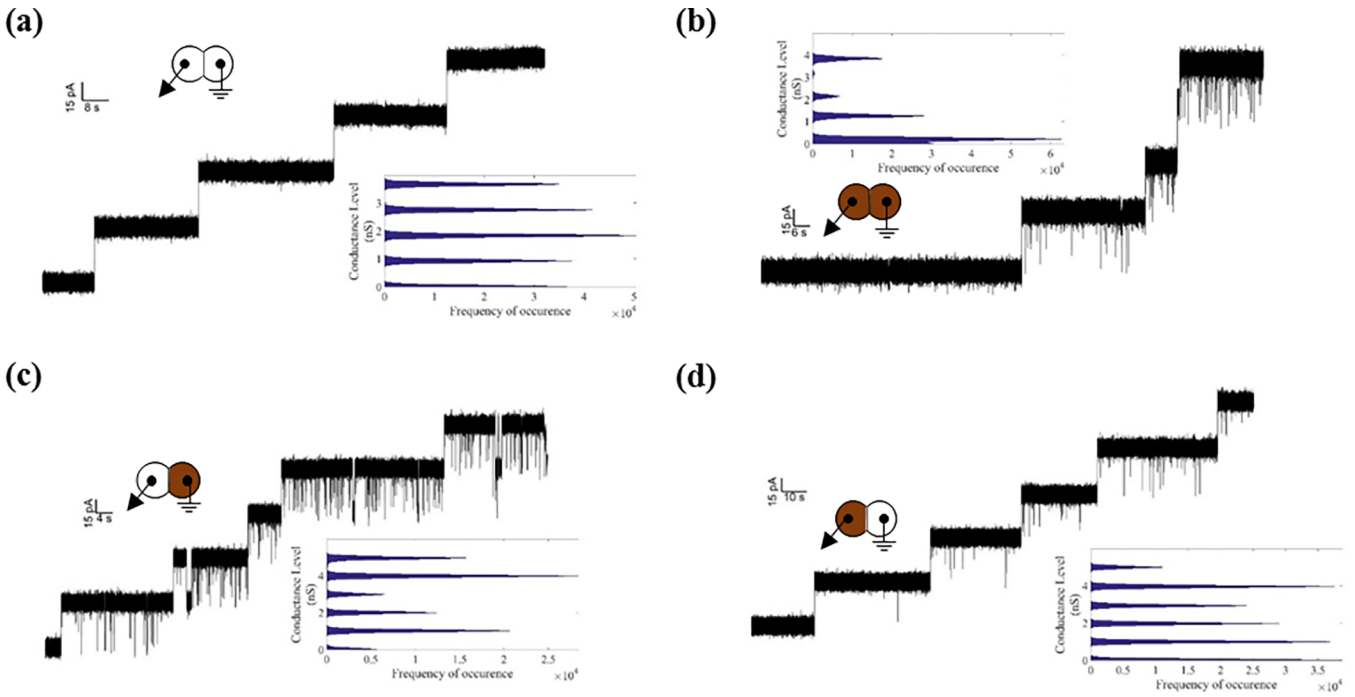

Figure 6. Alpha-hemolysin insertion activity is measured as stepwise increases in the current measured with a constant applied voltage of +50 mV. Panel a shows a typical scenario for a DIB formed between two water droplets. Panel b shows the observed αHL behavior for a membrane formed between two ferrofluid droplets. Mixed droplet behavior is presented in panels c and d, where a water and a ferrofluid droplet were combined. In all cases, αHL was added at a concentration of 1.25 μg/mL to the reference droplet. The obtained current traces were recorded in voltage clamp mode at a sampling frequency of 5 kHz and filtered and filtered at 1 kHz (using the embedded low-pass Bessel filter −80 dB/decade). Postacquisition, data was filtered at 500 Hz using a fourth order Butterworth low-pass filter in MATLAB. Possible blocking events occur whenever ferrofluid is being incorporated. However, all observed channel insertion events showed conductivities that fall within the acceptable reported range.

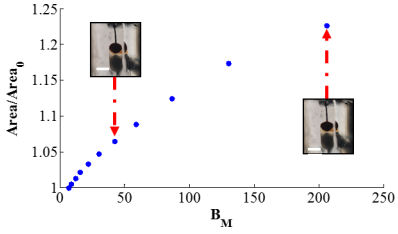

Figure 7. Magnetowetting or the control over the membrane area through a magnetic field was demonstrated by compressing a ferrofluid droplet into a hydrogel support. The proximity of the magnet was increased in a stepwise fashion of 1 mm per increment, and the membrane grew in response. When the permanent magnet was removed, the membrane resumed its original equilibrium dimensions. The ratio of the evolving membrane area with respect to its original area increases with an increasing magnetic Bond number as shown. The scale bars on the insets represent 1 mm.

a more flattened, cylindrical shape within the channel. The offset in the plot in the magnetic Bond number is due to the resolution of the experiment; perceptible changes in membrane area did not occur when the magnet was moved further away. This behavior was reversible; once the magnet was removed, the membrane shrank back to its original dimensions. No perceptible changes in membrane area were observed for control cases with water droplets instead of ferrofluid droplets when the magnet was brought closer to the membrane.

CONCLUSIONS

The incorporation of ferrofluids within the aqueous phases of the droplet interface bilayer technique for the repetitive assembly of functional and stable bilayer networks was investigated. Our analysis has shown that the functionality of the membranes was not significantly altered by the presence of the magnetic fluid. Bilayers formed between magnetically responsive droplets exhibit properties (specific capacitance, contact angle, monolayer tension, bilayer tension, and energy of adhesion) that fall within the range of their nonmagnetic counterparts. Droplet−droplet transport can still be established through αHL pores, further increasing the potential uses of ferrofluids within DIB-based materials. Ferrofluids allow for contact-free manipulation of membrane properties such as dynamic tuning of membrane properties through externally supplied magnetic fields while retaining the classic functionalities of DIB networks. Building more complex 3D bilayer networks with incorporated ferrofluid droplets is a promising step toward the creation of magnetically responsive and reconfigurable droplet networks.

AUTHOR INFORMATION

Corresponding Author

*E-mail: ecfreema@uga.edu.

ORCID

Eric C. Freeman: 0000-0003-1209-9813

Notes

The authors declare no competing financial interest.

ACKNOWLEDGMENTS

M.M.-M. and E.F. graciously acknowledge support from the National Science Foundation (NSF) under Grant #1537410. W.Z. and L.M. acknowledge support from NSF Grant #1150042. N.G. and C.O. were supported by a NSF REU

DOI: 10.1021/acs.langmuir.7b03055
Langmuir 2017, 33, 13000−13007

site program under Grant #1359095. J.N. acknowledges support from Air Force Office of Scientific Research (AFOSR) Grant # FA9550-12-1-0464. All experiments and analyses were conducted at the University of Georgia.

REFERENCES

(1) Hwang, W. L.; Holden, M. A.; White, S.; Bayley, H. Electrical Behavior of Droplet Interface Bilayer Networks: Experimental Analysis and Modeling. *J. Am. Chem. Soc.* **2007**, *129* (38), 11854−11864.
(2) Bayley, H.; Cronin, B.; Heron, A.; Syeda, M. A. H. W. L. H. R.; Thompson, J.; Wallace, M. Droplet Interface Bilayers. *Mol. BioSyst.* **2008**, *4* (12), 1191−1208.
(3) Hwang, D. K.; Dendukuri, D.; Doyle, P. S. Microfluidic-based synthesis of non-spherical magnetic hydrogel microparticles. *Lab Chip* **2008**, *8* (10), 1640−1647.
(4) Funakoshi, K.; Suzuki, H.; Takeuchi, S. Lipid bilayer formation by contacting monolayers in a microfluidic device for membrane protein analysis. *Anal. Chem.* **2006**, *78* (24), 8169−8174.
(5) Holden, M. A.; Needham, D.; Bayley, H. Functional bionetworks from nanoliter water droplets. *J. Am. Chem. Soc.* **2007**, *129* (27), 8650−8655.
(6) Maglia, G.; Heron, A. J.; Hwang, W. L.; Holden, M. A.; Mikhailova, E.; Li, Q.; Cheley, S.; Bayley, H. Droplet networks with incorporated protein diodes show collective properties. *Nat. Nanotechnol.* **2009**, *4*, 437−440.
(7) Najem, J. S.; Dunlap, M. D.; Rowe, I. D.; Freeman, E. C.; Grant, J. W.; Sukharev, S.; Leo, D. J. Activation of bacterial channel MscL in mechanically stimulated droplet interface bilayers. *Sci. Rep.* **2015**, *5*, 13726.
(8) Freeman, E. C.; Najem, J. S.; Sukharev, S.; Philen, M. K.; Leo, D. J. The mechanoelectrical response of droplet interface bilayer membranes. *Soft Matter* **2016**, *12*, 3021−3031.
(9) Gross, L. C.; Heron, A. J.; Baca, S. C.; Wallace, M. I. Determining membrane capacitance by dynamic control of droplet interface bilayer area. *Langmuir* **2011**, *27* (23), 14335−42.
(10) Gross, L. C.; Castell, O. K.; Wallace, M. I. Dynamic and reversible control of 2D membrane protein concentration in a droplet interface bilayer. *Nano Lett.* **2011**, *11* (8), 3324−8.
(11) Leptihn, S.; Castell, O. K.; Cronin, B.; Lee, E. H.; Gross, L. C.; Marshall, D. P.; Thompson, J. R.; Holden, M.; Wallace, M. I. Constructing droplet interface bilayers from the contact of aqueous droplets in oil. *Nat. Protoc.* **2013**, *8* (6), 1048−57.
(12) Hwang, W. L.; Chen, M.; Cronin, B.; Holden, M. A.; Bayley, H. Asymmetric droplet interface bilayers. *J. Am. Chem. Soc.* **2008**, *130* (18), 5878−5879.
(13) Venkatesan, G. A.; Lee, J.; Farimani, A. B.; Heiranian, M.; Collier, C. P.; Aluru, N. R.; Sarles, S. A. Adsorption Kinetics Dictate Monolayer Self-Assembly for Both Lipid-In and Lipid-Out Approaches to Droplet Interface Bilayer Formation. *Langmuir* **2015**, *31* (47), 12883−12893.
(14) Bibette, J.; Calderon, F. L.; Poulin, P. Emulsions: basic principles. *Rep. Prog. Phys.* **1999**, *62* (6), 969.
(15) Leal-Calderon, F.; Schmitt, V.; Bibette, J. *Emulsion Science: Basic Principles*; Springer Science & Business Media: New York, 2007.
(16) Wauer, T.; Gerlach, H.; Mantri, S.; Hill, J.; Bayley, H.; Sapra, K. T. Construction and Manipulation of Functional Three-Dimensional Droplet Networks. *ACS Nano* **2014**, *8* (1), 771−779.
(17) Booth, M. J.; Schild, V. R.; Graham, A. D.; Olof, S. N.; Bayley, H. Light-activated communication in synthetic tissues. *Sci. Adv.* **2016**, *2* (4), e1600056.
(18) Sarles, S. A.; Leo, D. J. Physical encapsulation of droplet interface bilayers for durable, portable biomolecular networks. *Lab Chip* **2010**, *10* (6), 710−7.
(19) Sarles, S. A.; Leo, D. J. Membrane-based biomolecular smart materials. *Smart Mater. Struct.* **2011**, *20* (9), 094018.
(20) Nguyen, M. A.; Srijanto, B.; Collier, C. P.; Retterer, S. T.; Sarles, S. A. Hydrodynamic trapping for rapid assembly and in situ electrical characterization of droplet interface bilayer arrays. *Lab Chip* **2016**, *16* (18), 3576−88.
(21) Villar, G.; Graham, A. D.; Bayley, H. A tissue-like printed material. *Science* **2013**, *340* (6128), 48−52.
(22) Bayoumi, M.; Bayley, H.; Maglia, G.; Sapra, K. T. Multi-compartment encapsulation of communicating droplets and droplet networks in hydrogel as a model for artificial cells. *Sci. Rep.* **2017**, *7*, 45167.
(23) Dixit, S. S.; Pincus, A.; Guo, B.; Faris, G. W. Droplet Shape Analysis and Permeability Studies in Droplet Lipid Bilayers. *Langmuir* **2012**, *28* (19), 7442−7451.
(24) Lacasse, M.-D.; Grest, G. S.; Levine, D.; Mason, T.; Weitz, D. Model for the elasticity of compressed emulsions. *Phys. Rev. Lett.* **1996**, *76* (18), 3448.
(25) Mason, T.; Bibette, J. Shear rupturing of droplets in complex fluids. *Langmuir* **1997**, *13* (17), 4600−4613.
(26) Pollack, M. G.; Fair, R. B.; Shenderov, A. D. Electrowetting-based actuation of liquid droplets for microfluidic applications. *Appl. Phys. Lett.* **2000**, *77* (11), 1725−1726.
(27) Yamada, R.; Tada, H. Manipulation of Droplets by Dynamically Controlled Wetting Gradients. *Langmuir* **2005**, *21* (10), 4254−4256.
(28) Jiao, Z.; Huang, X.; Nguyen, N.-T.; Abgrall, P. Thermocapillary actuation of droplet in a planar microchannel. *Microfluid. Nanofluid.* **2008**, *5* (2), 205−214.
(29) Hao, P.; Lv, C.; Zhang, X.; Yao, Z.; He, F. Driving liquid droplets on microstructured gradient surface by mechanical vibration. *Chem. Eng. Sci.* **2011**, *66* (10), 2118−2123.
(30) Aghdaei, S.; Sandison, M. E.; Zagnoni, M.; Green, N. G.; Morgan, H. Formation of artificial lipid bilayers using droplet dielectrophoresis. *Lab Chip* **2008**, *8* (10), 1617−1620.
(31) Poulos, J. L.; Nelson, W. C.; Jeon, T.-J.; Kim, C.-J. C.; Schmidt, J. J. Electrowetting on dielectric-based microfluidics for integrated lipid bilayer formation and measurement. *Appl. Phys. Lett.* **2009**, *95* (1), 013706.
(32) Egatz-Gómez, A.; Melle, S.; García, A. A.; Lindsay, S. A.; Márquez, M.; Domínguez-García, P.; Rubio, M. A.; Picraux, S. T.; Taraci, J. L.; Clement, T.; Yang, D.; Hayes, M. A.; Gust, D. Discrete magnetic microfluidics. *Appl. Phys. Lett.* **2006**, *89* (3), 034106.
(33) Pipper, J.; Inoue, M.; Ng, L. F.; Neuzil, P.; Zhang, Y.; Novak, L. Catching bird flu in a droplet. *Nat. Med.* **2007**, *13* (10), 1259−63.
(34) Berthier, J. *Micro-drops and Digital Microfluidics*; William Andrew: Norwich, NY, 2012.
(35) Berthier, J.; Brakke, K. A. *The Physics of Microdroplets*; John Wiley & Sons: Hoboken, NJ, 2012.
(36) Zhao, W. J.; Zhu, T. T.; Cheng, R.; Liu, Y. F.; He, J.; Qiu, H.; Wang, L. C.; Nagy, T.; Querec, T. D.; Unger, E. R.; Mao, L. D. Label-Free and Continuous-Flow Ferrohydrodynamic Separation of HeLa Cells and Blood Cells in Biocompatible Ferrofluids. *Adv. Funct. Mater.* **2016**, *26* (22), 3990−3998.
(37) Berry, J. D.; Neeson, M. J.; Dagastine, R. R.; Chan, D. Y. C.; Tabor, R. F. Measurement of surface and interfacial tension using pendant drop tensiometry. *J. Colloid Interface Sci.* **2015**, *454*, 226−237.
(38) Miller, R.; Hofmann, A.; Hartmann, R.; Halbig, A.; Schano, K. H. Measuring dynamic surface and interfacial tensions. *Adv. Mater.* **1992**, *4* (5), 370−374.
(39) Girault, H.; Schiffrin, D.; Smith, B. Drop image processing for surface and interfacial tension measurements. *J. Electroanal. Chem. Interfacial Electrochem.* **1982**, *137* (2), 207−217.
(40) Cheng, P.; Li, D.; Boruvka, L.; Rotenberg, Y.; Neumann, A. Automation of axisymmetric drop shape analysis for measurements of interfacial tensions and contact angles. *Colloids Surf.* **1990**, *43* (2), 151−167.
(41) Hansen, F.; Rødsrud, G. Surface tension by pendant drop: I. A fast standard instrument using computer image analysis. *J. Colloid Interface Sci.* **1991**, *141* (1), 1−9.
(42) Lin, S.-Y.; Chen, L.-J.; Xyu, J.-W.; Wang, W.-J. An examination on the accuracy of interfacial tension measurement from pendant drop profiles. *Langmuir* **1995**, *11* (10), 4159−4166.

DOI: 10.1021/acs.langmuir.7b03055
Langmuir 2017, 33, 13000−13007

(43) Danelon, C.; Perez, J.-B.; Santschi, C.; Brugger, J.; Vogel, H. Cell membranes suspended across nanoaperture arrays. *Langmuir* **2006**, *22* (1), 22−25.
(44) Taylor, G. J.; Venkatesan, G. A.; Collier, C. P.; Sarles, S. A. Direct in situ measurement of specific capacitance, monolayer tension, and bilayer tension in a droplet interface bilayer. *Soft Matter* **2015**, *11* (38), 7592−605.
(45) Thiam, A. R.; Bremond, N.; Bibette, J. From stability to permeability of adhesive emulsion bilayers. *Langmuir* **2012**, *28* (15), 6291−8.
(46) Najem, J.; Dunlap, M.; Sukharev, S.; Leo, D. J. Mechanosensitive Channels Activity in a Droplet Interface Bilayer System. *MRS Online Proc. Libr.* **2014**, *1621*, 171−176.
(47) Bergeron, V. Forces and structure in thin liquid soap films. *J. Phys.: Condens. Matter* **1999**, *11* (19), R215.
(48) Bergeron, V.; Martin, J.; Vovelle, L. Interaction of droplets with a surface: impact and adhesion. *Agro Food Industry Hi-Tech* **1999**, *10* (5), 21−23.
(49) Bibette, J.; Morse, D. C.; Witten, T. A.; Weitz, D. A. Stability Criteria for Emulsions. *Phys. Rev. Lett.* **1992**, *69* (16), 2439−2442.
(50) White, S. H. A Study of Lipid Bilayer Membrane Stability Using Precise Measurements of Specific Capacitance. *Biophys. J.* **1970**, *10* (12), 1127−1148.
(51) Requena, J.; Haydon, D. A. The lippmann equation and the characterization of black lipid films. *J. Colloid Interface Sci.* **1975**, *51* (2), 315−327.
(52) Wobschall, D. Voltage dependence of bilayer membrane capacitance. *J. Colloid Interface Sci.* **1972**, *40* (3), 417−423.
(53) Valincius, G.; Heinrich, F.; Budvytyte, R.; Vanderah, D. J.; McGillivray, D. J.; Sokolov, Y.; Hall, J. E.; Lösche, M. Soluble amyloid β-oligomers affect dielectric membrane properties by bilayer insertion and domain formation: implications for cell toxicity. *Biophys. J.* **2008**, *95* (10), 4845−4861.
(54) Song, L.; Hobaugh, M. R.; Shustak, C.; Cheley, S.; Bayley, H.; Gouaux, J. E. Structure of Staphylococcal alpha -Hemolysin, a Heptameric Transmembrane Pore. *Science* **1996**, *274* (5294), 1859−1865.
(55) Gouaux, J. E.; Braha, O.; Hobaugh, M. R.; Song, L.; Cheley, S.; Shustak, C.; Bayley, H. Subunit stoichiometry of staphylococcal alpha-hemolysin in crystals and on membranes: a heptameric transmembrane pore. *Proc. Natl. Acad. Sci. U. S. A.* **1994**, *91* (26), 12828−12831.
(56) Holden, M. A.; Bayley, H. Direct introduction of single protein channels and pores into lipid bilayers. *J. Am. Chem. Soc.* **2005**, *127* (18), 6502−6503.
(57) Tsuji, Y.; Kawano, R.; Osaki, T.; Kamiya, K.; Miki, N.; Takeuchi, S. Droplet split-and-contact method for high-throughput transmembrane electrical recording. *Anal. Chem.* **2013**, *85* (22), 10913−10919.
(58) Jeong, D. W.; Jang, H.; Choi, S. Q.; Choi, M. C. Enhanced stability of freestanding lipid bilayer and its stability criteria. *Sci. Rep.* **2016**, *6*, 38158.
(59) Belmonte, G.; Cescatti, L.; Ferrari, B.; Nicolussi, T.; Ropele, M.; Menestrina, G. Pore formation by Staphylococcus aureus alpha-toxin in lipid bilayers. *Eur. Biophys. J.* **1987**, *14* (6), 349−358.
(60) Sarles, S. A.; Leo, D. J. Regulated attachment method for reconstituting lipid bilayers of prescribed size within flexible substrates. *Anal. Chem.* **2010**, *82* (3), 959−966.
(61) Zhu, G.-P.; Nguyen, N.-T.; Ramanujan, R. V.; Huang, X.-Y. Nonlinear deformation of a ferrofluid droplet in a uniform magnetic field. *Langmuir* **2011**, *27* (24), 14834−14841.
(62) Nguyen, N.-T. Deformation of ferrofluid marbles in the presence of a permanent magnet. *Langmuir* **2013**, *29* (45), 13982−13989.

DOI: 10.1021/acs.langmuir.7b03055
Langmuir 2017, 33, 13000−13007